PAPER

Organic solar cells using CVD-grown graphene electrodes

To cite this article: Hobeom Kim *et al* 2014 *Nanotechnology* **25** 014012

View the article online for updates and enhancements.

You may also like

- Efficient charge generation at low energy losses in organic solar cells: a key issues review
  Ye Xu, Huifeng Yao, Lijiao Ma et al.

- ITO with embedded silver grids as transparent conductive electrodes for large area organic solar cells
  Bhushan R Patil, Mina Mirsafaei, Pawe Piotr Cielecki et al.

- Efficient ternary organic solar cells with high absorption coefficient DIB-SQ as the third component
  Hui-Xin Qi, , Bo-Han Yu et al.

Recent citations

- Influence of the Underlying Substrate on the Physical Vapor Deposition of Zn-Phthalocyanine on Graphene
  Timothy Mirabito *et al*

- Engineering electrodes and metal halide perovskite materials for flexible/stretchable perovskite solar cells and light-emitting diodes
  Kyung-Geun Lim *et al*

- Organic solar cells: Current perspectives on graphenebased materials for electrodes, electron acceptors and interfacial layers
  Edigar Muchuweni *et al*

Organic solar cells using CVD-grown graphene electrodes

Hobeom Kim[1], Sang-Hoon Bae[2], Tae-Hee Han[1], Kyung-Geun Lim[1], Jong-Hyun Ahn[2] and Tae-Woo Lee[1]

[1] Department of Materials Science and Engineering, Pohang University of Science and Technology, Pohang 790-784, Korea
[2] School of Electrical and Electronic Engineering, Yonsei University, Seoul 120-749, Korea

E-mail: ahnj@yonsei.ac.kr and twlee@postech.ac.kr

Abstract

We report on the development of flexible organic solar cells (OSCs) incorporating graphene sheets synthesized by chemical vapor deposition (CVD) as transparent conducting electrodes on polyethylene terephthalate (PET) substrates. A key barrier that must be overcome for the successful fabrication of OSCs with graphene electrodes is the poor-film properties of water-based poly(3,4-ethylenedioxythiphene):poly(styrenesulfonate) (PEDOT:PSS) when coated onto hydrophobic graphene surfaces. To form a uniform PEDOT:PSS film on a graphene surface, we added perfluorinated ionomers (PFI) to pristine PEDOT:PSS to create 'GraHEL', which we then successfully spin coated onto the graphene surface. We systematically investigated the effect of number of layers in layer-by-layer stacked graphene anode of an OSC on the performance parameters including the open-circuit voltage (V_{oc}), short-circuit current (J_{sc}), and fill factor (FF). As the number of graphene layers increased, the FF tended to increase owing to lower sheet resistance, while J_{sc} tended to decrease owing to the lower light absorption. In light of this trade-off between sheet resistance and transmittance, we determined that three-layer graphene (3LG) represents the best configuration for obtaining the optimal power conversion efficiency (PCE) in OSC anodes, even at suboptimal sheet resistances. We finally developed efficient, flexible OSCs with a PCE of 4.33%, which is the highest efficiency attained so far by an OSC with CVD-grown graphene electrodes to the best of our knowledge.

S Online supplementary data available from stacks.iop.org/Nano/25/014012/mmedia

(Some figures may appear in colour only in the online journal)

1. Introduction

Recently developed organic solar cells (OSCs) with single or tandem structures [1–3] have attained power conversion efficiencies (PCEs) in excess of 10% and have attracted increasing attention for potential use in many kinds of electronic devices—in particular, mobile applications—owing not only to their high PCE but also to their light weight, flexibility, and large area, low-cost producibility. Based on its conductive properties and high transparency in the visible range, indium tin oxide (ITO) has conventionally been used as transparent conducting electrodes for OSCs; however, ITO has critical

drawbacks in terms of increasing cost and brittleness, making it unsuitable as a material for electrodes in flexible OSCs [4, 5]. There have, correspondingly, been many efforts to replace ITO in conventional electrodes with materials such as graphene, carbon nanotubes, silver nanowires, and conducting polymers [6–9]. Among these, graphene—a two-dimensional, single-atom-thick carbon sheet—has been proposed as a material for flexible, transparent OSC conducting electrodes in light of its excellent electrical, optical, and mechanical properties [10–12]. After Novoselov *et al* demonstrated fabrication of graphene flakes using scotch tape, various fabrication methods have been developed [10, 13–16].
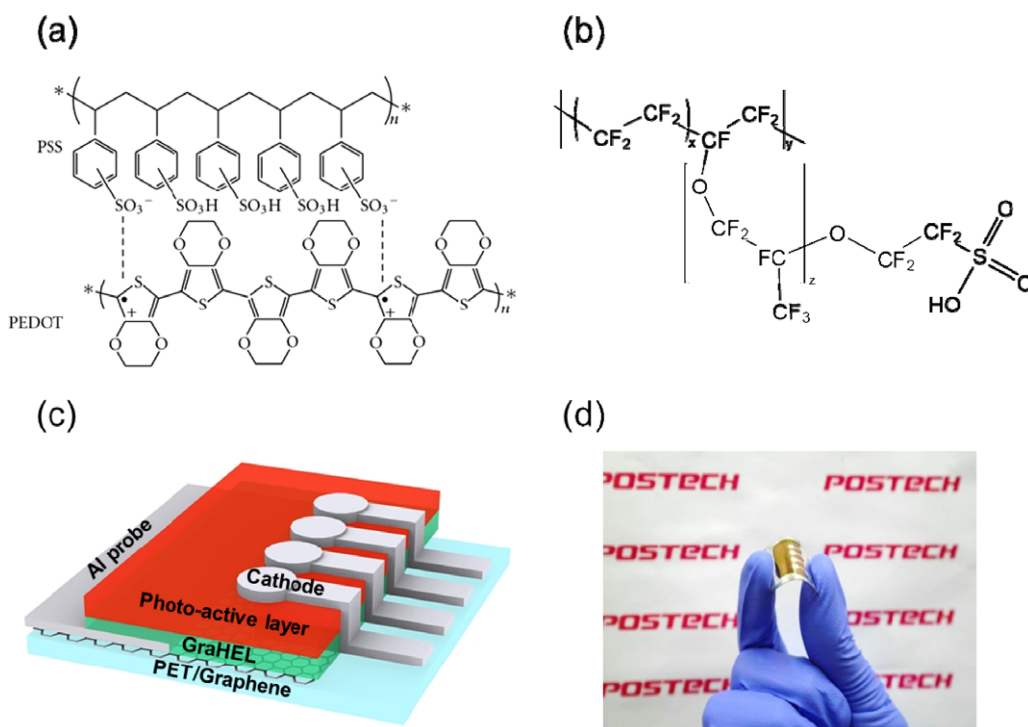
Figure 1. Molecular structures of (a) PEDOT:PSS and (b) tetrafluoroethylene-perfluoro-3,6-dioxa-4-methyl-7-octenesulfonic acid copolymer (PFI). (c) Schematic device configuration of the OSC device with graphene electrode on a PET substrate. (d) Optical image of a complete flexible OSC device incorporating a graphene electrode.

Most graphene sheets developed for OSC electrodes have either used reduced graphene oxide (rGO) or have been produced by chemical vapor deposition (CVD) methods, as these techniques are simpler in terms of synthesis and patterning and can maintain high uniformity over large areas [17–26]. However, when used as an OSC electrode material, rGO tends to suffer from structural defects that result in higher sheet resistance (R_{sh}) than—and therefore inferior performance to—CVD-grown graphene. Wu *et al* developed rGO films with $R_{sh} = 100$–500 kΩ/sq and transmittances of 85–95% for use as OSC electrodes and reported a PCE of 0.4% using a copper phthalocyanine (CuPC)/C_{60} bilayer as a photo-active layer [17]. Yin *et al* obtained a PCE of 0.78% and a transmittance of 65% from rGO electrodes with $R_{sh} = 3.2$ kΩ/sq using blended films of poly(3-hexylthiophene) (P3HT) and [6,6]-phenyl-C61-butyric acid methyl ester (PCBM) as a photo-active layer [18]. Several OSCs with CVD graphene electrodes have shown performance comparable to those with ITO electrodes, which can be mainly attributed to even lower R_{sh} values of CVD-grown graphene electrodes than those of rGO-based electrodes [20, 23, 25, 26]. Despite their high PCE, however, the development of OSCs with CVD graphene electrodes has faced considerable challenges in attempts at coating a layer of water-based poly(3,4-ethylenedioxythiphene):poly-(styrenesulfonate) (PEDOT:PSS), a material conventionally used as a hole extraction layer (HEL) in OSCs, as the hydrophobic nature of graphene makes it difficult to coat hydrophilic PEDOT:PSS onto its surface. To overcome this problem, significant efforts have been made in terms of

interface engineering between graphene and the HEL. In 2009, Loh *et al* modified a graphene surface with the self-assembled molecule pyrene butanoic acid succidymidyl ester (PBASE), allowing PEDOT:PSS to be coated onto the modified graphene film [19]. Then, in 2011, they used a thin (2 nm) MoO_3 layer to modify a graphene film in order to increase the wettability of PEDOT:PSS on the film [20]. Park *et al* introduced a method for coating PEDOT onto a graphene surface using vapor-phase polymerization instead of spin coating [25] and have recently further developed a method to modify a graphene surface with a double HEL [26]. All of these methods, however, require the use of an additional layer or set of processes to modify the graphene surface, which is far from a simple processing approach.

In this study, we synthesized monolayer graphene using a CVD method and stacked it layer-by-layer (LBL) for use as OSC electrodes. Prior to fabrication, we attempted to solve the problem of the poor wetting of hydrophilic PEDOT:PSS onto graphene surfaces. By blending pristine PEDOT:PSS with the less hydrophilic tetrafluoroethylene-perfluoro-3,6-dioxa-4-methyl-7-octenesulphonic acid copolymer (one of the perfluorinated ionomers (PFI)) to produce 'GraHEL', we enhanced the film coating quality of the hydrophobic graphene surface; figures 1(a) and (b) show the molecular structure of PEDOT:PSS and PFI, respectively. We then fabricated flexible OSCs with graphene anodes on poly(ethyleneterephthalate) (PET) substrates. Although considerable previous research has been conducted on OSCs with graphene electrodes, only two papers reported the effect of the thickness of graphene layers on the performance of OSCs [17, 18].

However, the authors of those papers did not use CVD-grown graphene as electrodes of OSCs but solution-processed rGO. Moreover, the overall photovoltaic parameters such as FFs and PCEs were so low that the tendency of device performance with a function of graphene thickness could not be clearly explained. Therefore, we systematically investigated how the change in the number of CVD-grown graphene layers affects open-circuit voltage (V_{oc}), short-circuit current (J_{sc}), fill factor (FF), and PCE separately. A schematic device configuration of the entire flexible device is shown in figures 1(c) and (d). In attempting to optimize the OSC performance, we found that there is a trade-off between R_{sh} and transmittance of the graphene film; as the number of graphene layers increases, the graphene sheet becomes more conductive, which increases FF but also obstructs light absorption, which in turn lowers J_{sc}. Based on this trade-off, an optimal number of graphene layers for an OSC should be found. We also demonstrated an efficient and flexible OSC with GraHEL using an efficient donor and acceptor system consisting of poly[*N*-9''-hepta-decanyl-2,7-carbazole-*alt*-5,5-(4', 7'-di-2-thienyl-2',1',3'-benzothiadiazole)] (PCDTBT) and [6,6]-phenyl-C71-butyric acid methyl ester ($PC_{70}BM$), respectively.

2. Experimental details

Graphene sheets were prepared using a well-known CVD method in which a Cu foil was inserted into a CVD furnace and heated up to 1000 °C with a H_2 gas inflow at 2 sccm. After annealing for an hour, CH_4 was added to the furnace at 1000 °C for an additional 30 min and then removed before the sample was rapidly cooled down to room temperature in the H_2 gas to complete the process. To create a transparent conducting electrode from the CVD-grown graphene, the Cu foil was etched by an etchant (CE-100, Transene), and the graphene was then transferred onto a polyethylene terephthalate (PET) substrate using a poly(methyl methacrylate) (PMMA) supporting layer. To achieve multilayer graphene films, the process above was repeated. A 100-nm-thick Al probe was thermally evaporated under high vacuum (5 × 10^{-7} Torr) onto the transferred graphene films in order to create electrical contacts for easier measurement and reduce the potential drop between the electrode probe and the defined photo-active region caused by the low sheet resistance of graphene. To avoid damaging the outermost graphene electrode layer from reactive ion etching, the O_2 plasma process previously used in patterning electrodes was removed because we used common graphene electrodes [7]. The graphene films on the PET substrates were p-doped with nitric acid (HNO_3) vapor for 90 s in order to lower their sheet resistance. After doping, the films were placed in high vacuum (5 × 10^{-7} Torr) for 3 h in order to remove physically adsorbed dopant molecules. Next, the doped graphene anode was UV-ozone treated for 10 min, and a GraHEL solution composed of PEDOT:PSS (Clevios PH H. C. Starck) and a PFI solution (tetrafluoroethyleneperfluoro-3,6-dioxa-4-methyl-7-octenesulphonic acid copolymer, CAS number 31175-20-9, Sigma-Aldrich) (PEDOT:PSS:PFI =

1:2.5:1.46 (by weight), water:alcohol ∼1:1 (by weight)), was spin coated onto the graphene surface at 1500 rpm for 90 s after filtration with a 0.45 μm polyvinylidene difluoride (PVDF) syringe filter. After spin coating, the GraHEL film was annealed on a hot plate in air at 150 °C for 30 min. Two different bulk heterojunction (BHJ) systems were used to develop an OSC photo-active layer. In one, 20 mg of poly(3-hexylthiophene) (P3HT) (Rieke Metals, P200) and 20 mg of 1-(3-methoxycarbonyl)-propyl-1-phenyl-(6,6)C61 (PCBM) (Nano-C) were dissolved together at a 1:1 weight ratio in 1 ml of 1,2-dichlorobenzene (DCB). After filtration with a 0.2 μm PTFE syringe filter, the completely dissolved solution was spin coated at 900 rpm for 5 s in a N_2 atmosphere, followed by solvent annealing in a glass Petri dish and thermal annealing at 150 °C for 30 min. The other photo-active layer was a BHJ film of poly[N-9''-hepta-decanyl-2,7-carbazole-alt-5,5-(4',7'-di-2-thienyl-2',1',3'-benzothiadiazole)] (PCDTBT) (1-material) and [6,6]-phenyl-C71-butyric acid methyl ester ($PC_{70}BM$) (EM-index). These were mixed at a weight ratio of 1:4, dissolved in DCB (35 mg ml^{-1}), and spin coated at 1600 rpm for 30 s onto the GraHEL in a N_2 atmosphere following filtration by a 0.45 μm PTFE syringe filter. After spin coating, the film was thermally annealed at 80 °C for 10 min. Finally, LiF/Al was deposited in 1 nm/100 nm layers onto the P3HT:PCBM system, and Ca/Al was deposited in 3 nm/100 nm layers onto the PCDTBT:$PC_{70}BM$ system by means of thermal evaporation under high vacuum (5 × 10^{-7} Torr). The completed devices were measured under a simulated air mass (AM) 1.5 with 100 mW cm^{-2} illumination.

3. Results and discussion

We compared the wettability of three different conducting polymer solutions (a pristine PEDOT:PSS solution, a mixture of PEDOT:PSS pristine solution and isopropyl alcohol (IPA) (1:1 w/w) (PHIPA), and a GraHEL solution) on graphene using contact angle measurements (figure 2). In the case of the pristine PEDOT:PSS dropped on a graphene surface, we observed large contact angle 75.4°, as the hydrophobic nature of graphene hinders this substance from wetting its surface; this suggests that pristine PEDOT:PSS cannot form a uniform film through spin coating onto a hydrophobic graphene surface. In contrast, both the PHIPA and GraHEL solutions, which contain IPA, were able to completely wet the graphene surface with contact angle values of 4.4° and 3.0° respectively. Because IPA is less polar than water, mixing it with the pristine water-dispersed PEDOT:PSS solution improved the wettability of these modified solutions on the non-polar graphene surface. In spite of the high wettability of the IPA-modified PEDOT:PSS (PHIPA) solutions, the problem of non-uniform spreading still arose when spin coating PHIPA onto the graphene surface (figure 2(d)). The GraHEL solution, however, fully covered the hydrophobic graphene surface (figure 2(f)). Thus, we were able to successfully fabricate OSCs by uniformly coating GraHEL onto the graphene electrodes.
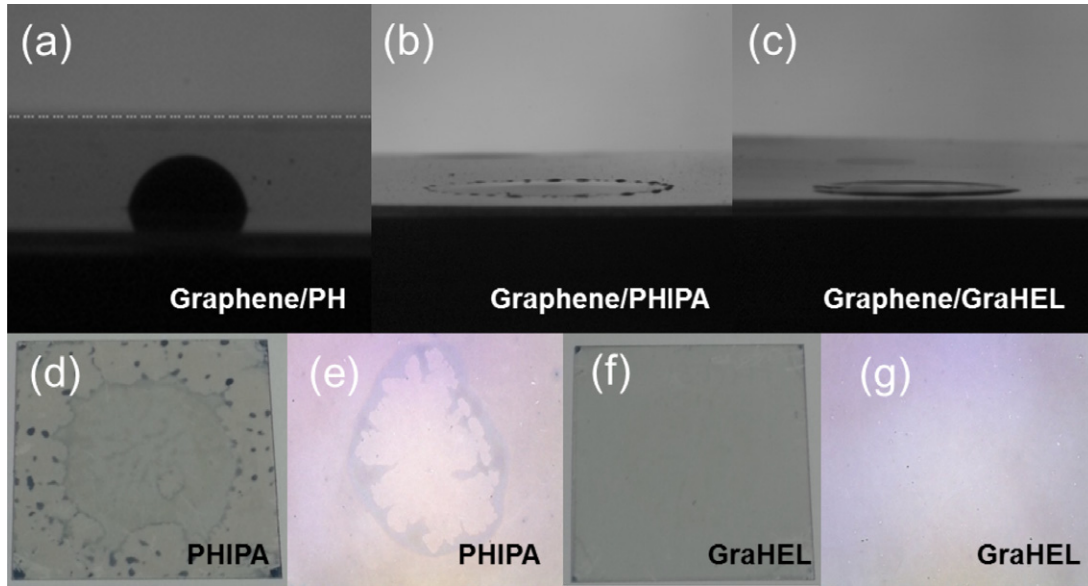
Figure 2. Contact angle images for various types of HTL materials: (a) graphene/PH (pristine PEDOT:PSS), (b) graphene/PHIPA (PH:IPA (1:1 by weight)), and (c) graphene/GraHEL (PH:IPA:PFI (8:8:1 by weight)). Optical images of spin coated (d) PHIPA and (f) GraHEL on a graphene surface. Enlarged optical microscopy images of (e) PHIPA and (g) GraHEL films on a graphene surface.
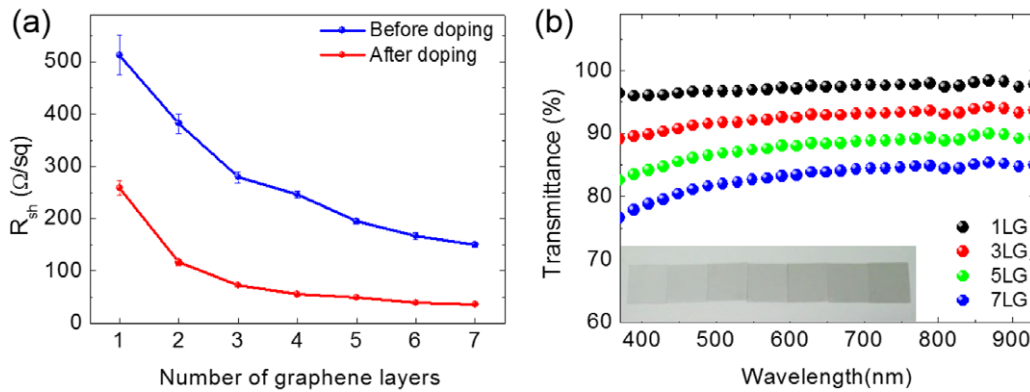

Figure 3. (a) Sheet resistance of graphene before and after HNO_3 doping as a function of the number of graphene layers. (b) UV–visible spectroscopy transmittance characteristics for 1, 3, 5, and 7LG. (Inset) Optical images of LBL stacked graphene on PET substrates from 1 layer (left) to 7 layers (right).

Table 1. Summary of the average sheet resistances of graphene layers before and after HNO_3 doping, as measured by a four-point probe. The number of graphene layers is varied from 1 to 7. (Note: measured over ten spots for the graphene films on PET; standard deviation in parentheses.)

	1L	2L	3L	4L	5L	6L	7L
Before doping R_{sh} (Ω/sq)	512.5 ($\pm$37.9)	382.2 ($\pm$19.0)	279.5 ($\pm$10.8)	246.5 ($\pm$6.3)	194.8 ($\pm$4.4)	166.8 ($\pm$6.9)	150.6 ($\pm$5.1)
After doping R_{sh} (Ω/sq)	258.6 ($\pm$13.9)	116.7 ($\pm$5.7)	72.9 ($\pm$3.4)	55.5 ($\pm$2.2)	49.7 ($\pm$1.5)	39.3 ($\pm$1.5)	36.6 ($\pm$0.7)

Figure 3(a) shows the values of R_{sh} of graphene films on a PET substrate measured with a four-point probe as a function of the number of layers; these values are also summarized in table 1. As previously discussed, R_{sh} tends to decrease as the number of LBL stacked graphene layers increases [7, 14, 15], and we observed this behavior in our experimental results in which R_{sh} continuously decreased without any additional chemical treatment from 512.5 to 150.6 Ω/sq for monolayer

graphene (1LG) to seven-layer graphene (7LG), respectively. After HNO_3 doping, R_{sh} for 7LG dramatically decreased to 36.6 Ω/sq, a value that is a little higher than or close to that of ITO at the same transmittance (for ITO, $R_{sh} \sim 10$ Ω/sq and transmittance $\sim$85% at 550 nm) [27]. It is well known that the transmittance of graphene decreases linearly by 2.3% for every layer that is stacked. To confirm this, we measured the transmittances of 1, 3, 5, and 7LG with UV–vis absorption
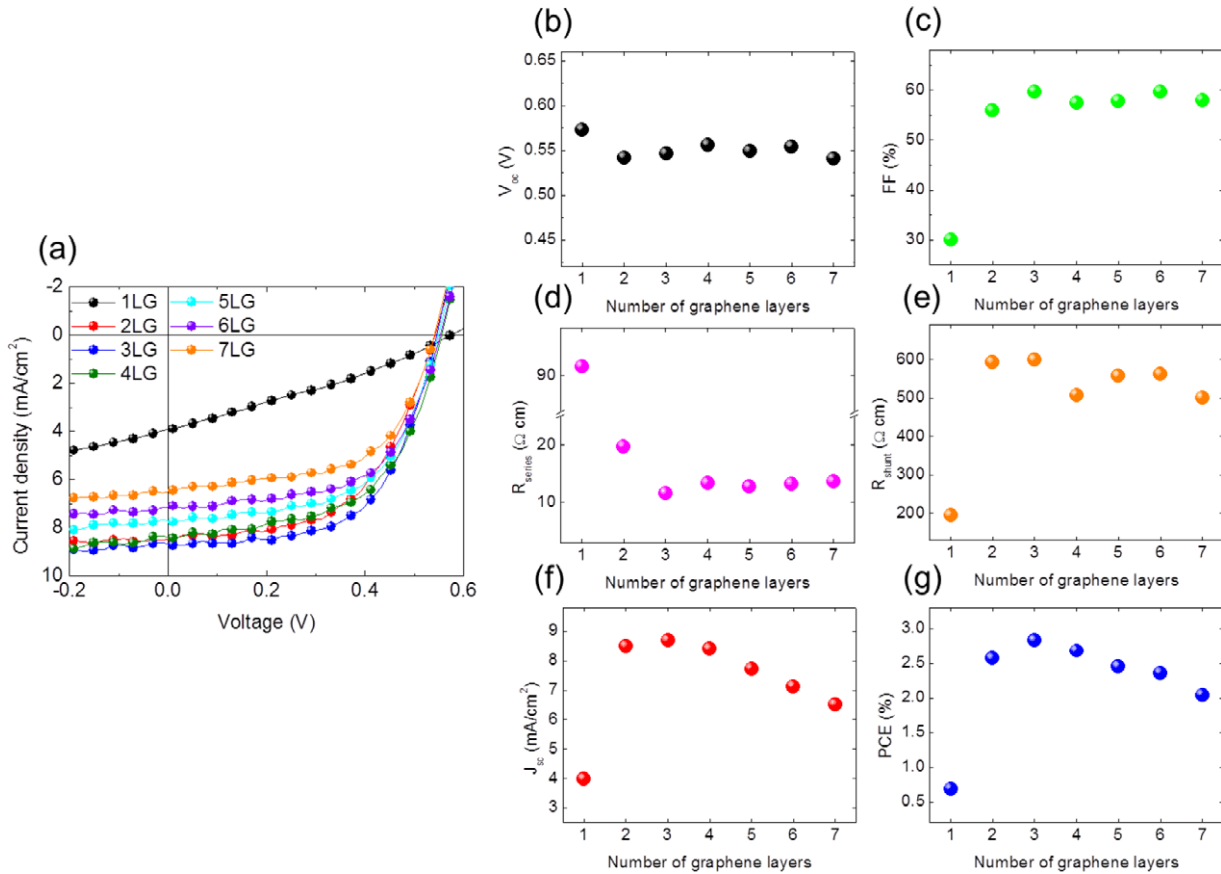
Figure 4. (a) *J–V* characteristics of OSCs with graphene electrodes for various numbers of graphene layers. Photovoltaic performance parameters: (b) V_{oc}, (c) FF, (d) R_{series}, (e) R_{shunt}, (f) J_{sc}, and (g) PCE for OSCs as the number of graphene layers is varied separately.

Table 2. Summary of the transmittances of the graphene layers at a wavelength of 550 nm.

	1L	3L	5L	7L
Transmittance (%)	96.8	92.1	87.5	82.8

spectroscopy and plotted the results in figure 3(b). The inset of the figure 3(b) shows the gradation of transmittance as the number of graphene layers increases from left (1LG) to right (7LG). These measured values agree closely with the literature [11]. The transmittance at a wavelength of 550 nm for each graphene layering is summarized in table 2.

To investigate the influence of the number of graphene layers on the performance parameters V_{oc}, J_{sc}, FF, series resistance (R_{series}), shunt resistance (R_{shunt}), and PCE of an OSC, we fabricated several OSCs with graphene anodes using a P3HT:PCBM blend as the photo-active layer. Figure 4 shows the current density–voltage (*J–V*) characteristics of OSCs with varying numbers of graphene electrode layers, with the various photovoltaic parameters (in sequence: V_{oc}, FF, R_{series}, R_{shunt}, J_{sc}, and PCE) plotted separately and the values of these parameters are summarized in table 3. As can be seen in figure 4(b), with the exception of the 1LG electrode device, all devices have nearly the same V_{oc} in the range between 0.54 and 0.55 V; this confirms that there is no change in the built-in potential of the device when increasing the number of graphene layers. The numerous defects that destroyed the atomic network of the 1LG graphene sheet likely resulted in the variance of its surface potential from that of graphene sheets with more layers [28, 29]; i.e., stacking additional graphene sheets above 1LG helps to relieve the effect of defects and thus consistently maintain V_{oc}. On the other hand, variations in FF and J_{sc}—and thus in PCE—were observed as a function of the number of graphene layers. In photovoltaic cells, FF is essentially determined by both R_{series} and R_{shunt} of a device, and we extracted these two resistances separately from the inverses of the slope of the *J–V* curves at the points V_{oc} and J_{sc}. In this case, the dominant factor affecting these two resistances is the R_{sh} of the graphene electrodes. The 1LG electrode device exhibited the lowest values for both FF and J_{sc} (figures 4(c) and (f)), which can be attributed to two facts: that this device had the highest electrode R_{sh} (258.6 Ω/sq), and thus the highest R_{series} (91.7 Ω cm), of all of the devices; and also that insufficient charge transfer occurred from the organic layers to the electrode owing to obstructions caused by numerous defects in the monolayer graphene on the PET substrate [28]. Thus, the significant leakage current likely caused by these defects was responsible for the 1LG having the lowest R_{shunt} (194.9 Ω cm). As is the case for V_{oc}, however, the poor J_{sc}, R_{series}, and R_{shunt} of the device can be alleviated by stacking more graphene layers in order to form more

Table 3. Summary of the performance of the OSCs in figure 4 for each graphene electrode.

The number of graphene layers (anode)	V_{oc} (V)	J_{sc} (mA cm^{-2})	FF (%)	PCE (%)	R_{series} (Ω cm)	R_{shunt} (Ω cm)
1	0.573	3.98	30.1	0.69	91.7	194.9
2	0.542	8.49	55.9	2.57	19.7	592.7
3	0.546	8.69	59.7	2.83	11.6	598.9
4	0.556	8.40	57.4	2.68	13.3	508
5	0.549	7.73	57.8	2.45	12.7	557.1
6	0.554	7.13	59.7	2.36	13.2	561.3
7	0.541	6.51	58.0	2.04	13.6	500.6

conductive electrodes and cover defects (figures 4(d) and (f)). The addition of a second monolayer graphene covering the underlying graphene layer and thereby significantly lowered R_{sh} (116.7 Ω/sq), making the 2LG capable of serving as an effective OSC anode, and using a 2LG sheet as an electrode, decreases R_{series} (to 19.7 Ω cm) and increases R_{shunt} (to 592.7 Ω cm) while dramatically increasing FF and J_{sc} to 55.9% and 8.49 mA cm^{-2}, respectively. The lowering of R_{sh} by adding graphene layers to increase FF and J_{sc} is observed in the 3LG sheet as well, with this device showing peak values of FF and J_{sc} of 59.7% and 8.69 mA cm^{-2}, respectively. However, as the number of graphene layers increased above three, J_{sc} started to decrease, while FF saturated with saturated R_{series} and R_{shunt}, as can be seen in figures 4(c) and (f). The saturation of FF in devices with a 3LG electrode means that the 3LG has an R_{sh} low enough for use as an electrode of an OSC device. It was clearly observed that J_{sc} decreased after saturation of FF, a result that can be attributed to the decrease in transmittance of the graphene sheets, as shown in figure 4(f); in other words, J_{sc} became the dominant factor for determining PCE after saturation of the FF. Consequently, the highest PCE of 2.83% for the P3HT:PCBM devices was achieved with a 3LG device (figure 4(g)), leading us to conclude that 3LG is the optimal layering for OSC electrodes. To enhance PCE of flexible OSCs with graphene anodes, we additionally fabricated OSCs using a more efficient BHJ system of PCDTBT:PC$_{70}$BM with optimized conditions as described in section 2. We were able to achieve efficient OSC device and the *J–V* characteristic of this is shown in figure 5. The device attained V_{oc} of 0.896 V, J_{sc} of 8.83 mA cm^{-2}, FF of 54.7%, and a PCE of 4.33%, which, to the best of our knowledge, represents the highest efficiency attained by an OSC with CVD-grown graphene electrodes.

4. Conclusion

In this study, we attempted to overcome the poor-film coating problem of water-based conducting polymer solutions (PEDOT:PSS) on graphene films produced by CVD method without using additional layers or processes. Having successfully achieved this using a GraHEL solution containing a less hydrophilic perfluorocarbon-based ionomer, we systematically studied the effects of changing the number of graphene layers on the performance parameters of an OSC. Comparing devices with 1LG up to 7LG electrodes, we demonstrated that FF tends to increase up to three layers
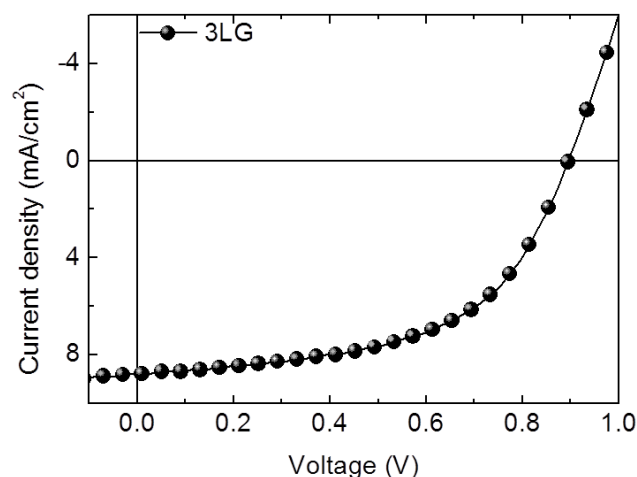

Figure 5. *J–V* characteristics of the OSC device with a 3LG electrode using a BHJ of PCDTBT:PC$_{70}$BM as a photo-active layer.

and then becomes saturated, while J_{sc} tends to decrease after three layers as a function of the number of additional layers. Based on trade-off between R_{sh} and transmittance of graphene films, we determined that 3LG electrodes optimized the OSC performance in terms of PCE; this result implies that a 3LG electrode has a sufficiently low R_{sh} after doping while maintaining a relatively high transmittance. Under optimal conditions, we fabricated a highly efficient OSC device with graphene anode that was able to attain a PCE of 4.33%.

Acknowledgments

References

[1] You J *et al* 2013 *Nature Commun.* **4** 1446
[2] www.heliatek.com/newscenter/
[3] Green M A, Emery K, Hishikawa Y, Warta W and Dunlop E D 2012 *Prog. Photovolt. Res. Appl.* **20** 12

[4] Kumar A and Zhou C 2010 *ACS Nano* **4** 11
[5] Hecht D S, Hu L and Irvin G 2011 *Adv. Mater.* **23** 1482
[6] Cai M, Ye Z, Xiao T, Liu R, Chen Y, Mayer R W, Biswas R, Ho K-M, Shinar R and Shinar J 2012 *Adv. Mater.* **24** 4337
[7] Han T-H, Lee Y, Chio M-R, Woo S-H, Bae S-H, Hong B H, Ahn J-H and Lee T-W 2012 *Nature Photon.* **6** 105
[8] Rowell M W, Topinka M A, McGehee M D, Prall H and Dennler G 2006 *Appl. Phys. Lett.* **88** 233506
[9] Jin J, Lee J, Jeong S, Yang S, Ko J-H, Im H-G, Baek S-W, Lee J-Y and Bae B-S 2013 *Energy Environ. Sci.* **6** 1811
[10] Novoselov K S, Geim A K, Morozov S V, Jiang D, Zhang Y, Dubonos S V, Grigorieva I V and Firsov A A 2004 *Science* **306** 666
[11] Nair R R, Blake P, Grigorenko A N, Novoselov K S, Booth T J, Stauber T, Peres N M R and Geim A K 2008 *Science* **320** 1308
[12] Lee C, Wei X, Kysar J W and Hone J 2008 *Science* **321** 385
[13] Eda G, Fanchini G and Chhowalla M 2008 *Nature Nanotechnol.* **3** 270
[14] Kim K S, Zhao Y, Jang H, Lee S Y, Kim J M, Kim K S, Ahn J-H, Kim P, Choi J-Y and Hong B H 2009 *Nature* **457** 706
[15] Bae S *et al* 2010 *Nature Nanotechnol.* **5** 574
[16] Berger C *et al* 2006 *Science* **312** 1191

[17] Wu J, Becerril H A, Bao Z, Liu Z, Chen Y and Peumans P 2008 *Appl. Phys. Lett.* **92** 263302
[18] Yin Z, Sun S, Salim T, Wu S, Huang X, He Q, Lam Y M and Zhang H 2010 *ACS Nano* **4** 5263
[19] Wang Y, Chen X, Zhong Y, Zhu F and Loh K P 2009 *Appl. Phys. Lett.* **95** 063302
[20] Wang Y, Tong S W, Xu X F, Özyilmaz B and Loh K P 2011 *Adv. Mater.* **23** 1514
[21] Park H, Rowehl J A, Kim K K, Bulovic V and Kong J 2010 *Nanotechnology* **21** 505204
[22] Lee S, Yeo J-S, Cho C, Kim D-Y, Na S-I, Lee B H and Lee T 2012 *Nanotechnology* **23** 344013
[23] De Arco L G, Zhang Y, Schlenker C W, Ryu K, Thompson M E and Zhou C 2010 *ACS Nano* **4** 2865
[24] Park H, Brown P R, Bulovic V and Kong J 2012 *Nano Lett.* **12** 133
[25] Park H, Howden R M, Barr M C, Bulovic V, Gleason K and Kong J 2012 *ACS Nano* **6** 6370
[26] Park H, Chang S, Smith M, Gradecak S and Kong J 2013 *Sci. Rep.* **3** 1581
[27] De S and Coleman J N 2010 *ACS Nano* **4** 2713
[28] Banhart F, Kotakoski J and Krasheninnikov A V 2011 *ACS Nano* **5** 26
[29] Huang P Y *et al* 2011 *Nature* **469** 389